MSc Thesis

Estimation of Atrial Fibre Directions Based on Epicardial Electrograms

Johannes Willem de Vries

TUDelft

Estimation of Atrial Fibre Directions Based on Epicardial Electrograms

Thesis

submitted in partial fulfilment of the
requirements for the degree of

Master of Science

in

Electrical Engineering

by

Johannes Willem de Vries
born in Dordrecht, The Netherlands

This work was performed in:

Circuits and Systems Group
Department of Microelectronics
Faculty of Electrical Engineering, Mathematics and Computer Science
Delft University of Technology

Delft University of Technology

DELFT UNIVERSITY OF TECHNOLOGY
DEPARTMENT OF
MICROELECTRONICS

The undersigned hereby certify that they have read and recommend to the Faculty of Electrical Engineering, Mathematics and Computer Science for acceptance a thesis entitled **"Estimation of Atrial Fibre Directions Based on Epicardial Electrograms"** by **Johannes Willem de Vries** in partial fulfilment of the requirements for the degree of **Master of Science**.

Dated: 27 June 2022

Chairman:

_____

dr.ir. R.C. Hendriks

Committee Members:

_____

dr. D.M.J. Tax

_____

dr.ir. R. Heusdens

_____

Miao Sun MSc

Abstract

Being able to estimate atrial tissue conductivity parameters from epicardial electrograms is an important tool in diagnosing and treating heart rhythm disorders such as atrial fibrillation. One of these parameters is the atrial fibre direction, which is often assumed to be known in conductivity estimation methods. In this thesis, a novel method to estimate the fibre direction from epicardial electrograms is presented. This method is based on local conduction slowness vectors of a propagating activation wave, which can be calculated from a corresponding activation map of the atrial tissue. These conduction slowness vectors follow an elliptical pattern that strongly depends on the underlying conductivity parameters. The fibre direction and conductivity anisotropy ratio can therefore be estimated by fitting an ellipse to the conduction slowness vectors. Applying the presented method on simulated data shows that it can accurately estimate the fibre direction, and that the performance of the method depends mostly on the range of wavefront directions present in the measurement area. The main advantage of the presented method over existing methods is that it still functions in the presence of conduction blocks, as long as the surrounding tissue is approximately homogeneous.

Preface

This master thesis is the culmination of an eight months long graduation project, written in order to obtain the degree of master of science in electrical engineering. The graduation project was performed under the Circuits and Systems Group at Delft University of Technology, and expands upon the several projects on atrial fibrillation and epicardial electrograms. Preceding the graduation project, a two months long literature review was carried out as an extra project. The report that resulted is largely absorbed into the introductory chapters, and is therefore not appended to this thesis.

On 1 and 2 June 2022, the 42nd WIC Symposium on Information Theory and Signal Processing in the Benelux (SITB 2022) took place. For this conference, I wrote an extended abstract about the findings of the graduation project. The abstract was accepted and a poster presentation was subsequently held on 1 June. Included in the appendix is a copy of the extended abstract that was submitted.

Finally, I would like to express my gratitude to my supervisors Richard Hendriks and Miao Sun for their guidance during the whole graduation project; your insight and involvement were invaluable. I also want to thank David Tax and Richard Heusdens for complementing the thesis committee. A special thanks goes out to my family and friends, who supported me and kept me motivated throughout the project duration.

Jordi de Vries
Delft, June 2022

Contents

Nomenclature

Abbreviations

AF	Atrial fibrillation.
CFA	Confirmatory factor analysis.
CMM	Compact matrix model.
ECG	Electrocardiogram.
EGM	(Epicardial) electrogram.
FDM	Finite difference method.
SCFA	Simultaneous confimatory factor analysis.

Symbols

C	Membrane capacitance per unit area.
I	Transmembrane current density.
I_{ion}	Total ionic current density.
I_{st}	Stimulus current density.
M	Total number of electrodes.
m	Electrode index.
N	Total number of nodes (cells).
n	Node (cell) index.
r	Cell to sensor distance.
s	Conduction slowness.
s_ℓ	Conduction slowness in longitudinal direction.
T	Total number of time instances.
t	Time index.
V	Transmembrane potential.
x	First spatial dimension index.
y	Second spatial dimension index.
z	Cell to sensor height.
α_s	Conduction slowness anisotropy ratio.
α_σ	Conductivity anisotropy ratio.
β	Cellular surface to volume ratio.
Δt	Sample time.
Δx	Distance between nodes in x-direction.
Δy	Distance between nodes in y-direction.
δ	Dirac delta function.
ζ	Fibre direction, longitudinal conductivity angle.
ξ	Longitudinal conduction slowness angle.
Σ	Conductivity tensor.
σ_{e}	Extracellular conductivity constant.
σ_ℓ	Conductivity in longitudinal direction.
τ	Local activation time.
Φ	Measured potential.

1

Introduction

Contractions of the heart are induced by action potentials propagating through the cardiac tissue. These action potentials consist of a rapid depolarisation of the transmembrane potential of a muscle cell (myocyte), causing the muscle to contract and the neighbouring cells to depolarise as well. The electrical propagation through the cardiac cells that follows is determined by the tissue conductivity. Due to the complex composition of cardiac tissue, the conductivity is generally inhomogeneous and orthotropic, with the main direction of propagation aligned with the fibre direction.

Impaired electrical conductivity in pathological tissue plays an important role in medicine as it gives rise to heart rhythm disorders such as atrial fibrillation (AF) [1]. The impaired conductivity hinders a smooth contraction of the atria, which has several long-term health risks such as an increased risk of heart failure and stroke. One of the ultimate steps of AF management is catheter ablation, a surgical procedure that can be performed to remove pathological spots in the tissue. An epicardial electrogram (EGM) is used to localise the these pathological spots, known as conduction blocks. Being able to estimate the local atrial tissue conductivity from EGM recordings is therefore an important tool in diagnosing and treating AF.

The inverse problem of estimating local tissue conductivity parameters from EGM measurements, however, is an ill-posed and highly challenging task due to high dimensionality, nonlinearity and stochasticity. Furthermore, most estimation approaches focus on finding only a single set of homogeneous parameters for the whole tissue, which does not facilitate localisation of areas with impaired conductivity. Recently, some methods have been developed that estimate conductivity parameters locally for groups of cells within the measurement area. Although these methods perform relatively well, they depend on a number of parameters that are assumed to be known. One of these parameters is the fibre direction, which influences the effective conductivity due to the orthotropic nature of the tissue. In this thesis, the effects of the fibre direction on the atrial physiology and on conductivity estimation are investigated, and methods to estimate the fibre direction for tissue with conduction blocks are explored.

The remainder of this thesis is organised as follows. Chapter 2 provides the relevant background information on the physiology of the heart as well as on the mathematical models that are commonly used to describe this physiology. This chapter also highlights two recent conductivity estimation methods. In Chapter 3, the effects of the fibre direction on the atrial physiology and on conductivity estimation are investigated. Using this knowledge, estimation of the fibre direction based on EGM measurements is explored in Chapter 4. Finally, Chapter 5 concludes the thesis and presents an overview of open questions and recommendations.

2

Background Knowledge

Cardiac tissue parameter estimation methods start with a mathematical model of the physiology of the heart. This chapter provides the necessary background information on this physiology. Different mathematical models on cell and tissue scale are highlighted as well. Finally, a selection of parameter estimation techniques are discussed. A more detailed overview of the cardiac physiology can be found in [2].

2.1. Physiology of the Heart

The heart is a muscular organ that is responsible for circulating blood through the body. The human heart consists of four chambers: the two upper atria where blood enters the heart and the two lower ventricles where blood is pumped out. All chambers are surrounded by cardiac tissue that provides mechanical contraction when stimulated electrically. The fibrous skeleton of the heart provides structure and serves as electrical boundary between chambers.

Cardiac tissue is a composite tissue and consists mainly of myocytes and fibroblasts. An extracellular matrix provides support to these cells and extracellular liquid fills the space in between. Fibroblasts are the most prominent cell type by number. Their main function is to maintain the extracellular matrix, but their effect on large scale electrical properties is not yet well understood [3]. Myocytes are the most prominent cell type by volume. Myocytes are muscle cells, capable of providing tension. The geometry of these cells can be approximated by a cylinder with a length of 50 to 150 µm and a diameter of 10 to 20 µm, but the true shapes and dimensions are highly variable throughout the tissue. Myocytes are typically joined at their ends such that the local fibre orientation can be defined along the longitudinal axes of the myocytes. Sheets consisting of 4 to 6 layers of myocytes are separated by cleavage planes and connective tissue, forming a laminar structure.

The interior of a myocyte is contained by a lipid membrane with an approximate capacitance of 1 to $10\,\mu\mathrm{F/cm}^2$. This membrane is responsible for governing the concentrations of different ions inside the cell. At rest, the principal intracellular ion is potassium (K^+) and the principal extracellular ions are sodium (Na^+) and chloride (Cl^-). The resulting electrical potential difference across the membrane, known as the transmembrane potential, is typically around $-81.2\,\mathrm{mV}$ at rest. The flow of these ions through the membrane is controlled by ion channels that gate the diffusion flow of specific ions, and ion pumps that move ions against the concentration gradient. These channels and pumps can be dependent on the intra- and extracellular concentrations of certain ions and on the transmembrane potential. Most ion channels are found at the ends of myocytes, such that electrical conductivity is higher along the longitudinal direction opposed to the transverse direction. Due to the laminar structure of the tissue, conductivity is lowest in the direction normal to the sheets. This makes conductivity an orthotropic tissue parameter with an experimentally found conductivity ratio approximately $4:2:1$ in longitudinal direction, transverse direction along the sheets and in direction normal to the sheets respectively [4].

Myocyte contraction is triggered by electrical depolarisation. Specialised myocytes in the sinoatrial node can generate an electrical impulse: the action potential. This action potential consists of a rapid depolarisation followed by a slower repolarisation. Figure 2.1 shows a typical action potential shape. The rapid depolarisation causes calcium (Ca^{2+}) to be released into the myocyte, which in turn causes
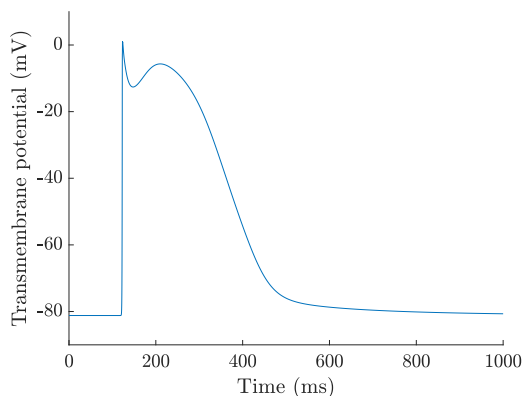
Figure 2.1: Typical simulated action potential at a cell, for a single heartbeat.
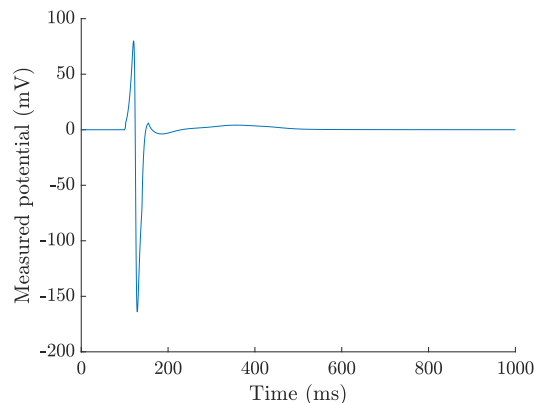
Figure 2.2: Example of a simulated unipolar EGM from an electrode, for a single heartbeat.

contraction. Due to intercellular coupling, depolarisation also induces depolarisation in neighbouring myocytes. Because of the delay in this coupling, each myocyte activates at a different time, known as the local activation time. A propagating depolatisation wave follows through the tissue. The orthotropic nature of the tissue conductivity means that the conduction velocity of the wave is also orthotropic and the wavefrons are therefore usually elliptical in shape. Figure 3.1 shows some examples of activation maps.

Different methods exist to measure the transmembrane potential of cardiac tissue. The most common method is electrocardiography, which uses electrodes that measure skin potential. The conventional setup consists of ten electrodes placed on the arms, legs and chest. This results in twelve measured potential differences known as leads, together forming the electrocardiogram (ECG). ECGs are relatively easy to make and do not require invasive surgery. Another approach is to place a high resolution electrode array on the surface of cardiac tissue during open heart surgery, and measure the potential at multiple locations simultaneously. The resulting measurements are known as an epicardiac electrogram (EGM). Although EGMs are more difficult to record, the benefit is that they can provide information on locally varying tissue parameters such as the conductivity. Figure 2.2 shows an example of an EGM from a single electrode.

2.2. Mathematical Models

Mathematical models of cardiac electrophysiology provide a simplified description of the complicated action potential propagation system. Most models are composed of a single cell model that details the ionic currents through the cell membrane, and a domain model that expands the single cell model to tissue scale. An EGM model provides the relationship between the transmembrane potential and measured potential.

Ionic Current Model

Different models of ionic current exist, most derived from experimental observations following the approaches pioneered by Hodgkin and Huxley [5]. Different models consider different types of cardiac cells and different mammalian species. An overview of cardiac cell models can be found in [6], [7].

For human atrial cells, a prominent model is the Courtemanche model published in 1998 [8]. This model decomposes the total ionic current through the membrane I_{ion} into twelve currents, each concerning a specific ion channel or pump. The gating properties of these channels and pumps are determined by in total 21 variables that follow temporal differential equations. These 21 variables include the transmembrane potential V, intracellular concentrations of Na^+ and K^+, the Ca^{2+} concentration in three different intracellular regions, and 15 gating variables that represent the probability of finding an ion channel open.

Domain Models

An ionic current model can be extended to tissue level by approximating the tissue as continuous and homogeneous. In the bidomain model, two overlapping domains separated by a membrane are considered: one for the intracellular and one for the extracellular space. Each domain is characterised by a location dependent conductivity tensor $\mathbf{\Sigma}_{\mathrm{i,e}}$, and potential $V_{\mathrm{i,e}}$ such that the transmembrane potential can be defined as

$$V = V_{\mathrm{i}} - V_{\mathrm{e}}. \tag{2.1}$$

Combining Ohm's law and conservation of current, the total outward transmembrane current density I can be expressed as

$$\begin{cases} I = \beta^{-1} \boldsymbol{\nabla}^{\mathrm{T}} \mathbf{\Sigma}_{\mathrm{i}} \boldsymbol{\nabla} V_{\mathrm{i}} \\ I = -\beta^{-1} \boldsymbol{\nabla}^{\mathrm{T}} \mathbf{\Sigma}_{\mathrm{e}} \boldsymbol{\nabla} V_{\mathrm{e}} \end{cases} \tag{2.2}$$

where β is a parameter representing the cellular surface to volume ratio. The transmembrane current density is composed of a capacitive current density from the cell membrane with capacitance per unit area C, and an ionic current density I_{ion} that follows from an individual cell model [5]. An external stimulus current density I_{st} can also be included, resulting in

$$I = C\frac{\partial V}{\partial t} + I_{\mathrm{ion}} - I_{\mathrm{st}}. \tag{2.3}$$

Combining (2.1), (2.2) and (2.3) leads to the two partial differential equations that constitute the bidomain model:

$$\begin{cases} \beta^{-1} \boldsymbol{\nabla}^{\mathrm{T}} \mathbf{\Sigma}_{\mathrm{i}} \boldsymbol{\nabla} (V + V_{\mathrm{e}}) = C\frac{\partial V}{\partial t} + I_{\mathrm{ion}} - I_{\mathrm{st}} \\ \boldsymbol{\nabla}^{\mathrm{T}} (\mathbf{\Sigma}_{\mathrm{i}} + \mathbf{\Sigma}_{\mathrm{e}}) \boldsymbol{\nabla} V_{\mathrm{e}} = -\boldsymbol{\nabla}^{\mathrm{T}} \mathbf{\Sigma}_{\mathrm{i}} \boldsymbol{\nabla} V. \end{cases} \tag{2.4}$$

Although the bidomain description of cardiac tissue is relatively accurate and reliable, finding numerical solutions can be challenging. A simplification to the bidomain model can be made by assuming that the intracellular and extracellular spaces have the same anisotropy such that the conductivity tensors are proportional. The cardiac tissue can then be considered as a single domain with conductivity tensor $\mathbf{\Sigma}$ that equals the two domain conductivities in series. Substituting this series conductivity into (2.4) then gives the transmembrane current density as

$$I = \beta^{-1} \boldsymbol{\nabla}^{\mathrm{T}} \mathbf{\Sigma} \boldsymbol{\nabla} V \tag{2.5}$$

which, combined with (2.3), yields

$$\beta^{-1} \boldsymbol{\nabla}^{\mathrm{T}} \mathbf{\Sigma} \boldsymbol{\nabla} V = C\frac{\partial V}{\partial t} + I_{\mathrm{ion}} - I_{\mathrm{st}}. \tag{2.6}$$

This single partial differential equation describes the monodomain model.

Because of the reduced number of partial differential equations, numerical solutions are easier to find for the monodomain model compared to the bidomain method. Furthermore, it has been shown that the monodomain model is still a good approximation of the bidomain model, even for unequal anisotropy ratios [9]–[11]. This only holds, however, as long as there is no injection of extracellular current involved, as is for example the case in defibrillation modelling.

These continuous domain models are often discretised for computational purposes. The tissue can be approximated by a regular lattice of $N_x \times N_y = N$ nodes that can either represent cells or groups of cells. The distance between nodes is denoted as Δx and Δy in the respective directions. Assuming a regular lattice allows for the finite difference method (FDM) to be used in place of continuous partial derivatives. Time can similarly be discretised with a period of Δt between samples.

Conductivity Tensor

The conductivity tensor is an important tissue parameter that relates currents through the tissue to the potential. Due to the orthotropic nature of the tissue, the eigenvectors of the conductivity tensor are
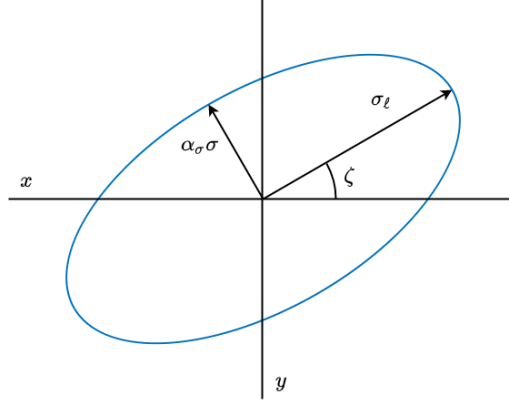
Figure 2.3: Ellipse representation of a conductivity tensor for a single node, with $\alpha_\sigma = \frac{1}{2}$ and $\zeta = \frac{1}{6}\pi$ rad.

orthonormal and the tensor is therefore always symmetric. When considering two dimensional tissue, the conductivity tensor is a 2×2 matrix and can generally be expressed as

$$\mathbf{\Sigma} = \begin{pmatrix} \sigma_{xx} & \sigma_{xy} \\ \sigma_{xy} & \sigma_{yy} \end{pmatrix}. \tag{2.7}$$

A more intuitive interpretation follows from applying an eigendecomposition

$$\mathbf{\Sigma} = \begin{pmatrix} \cos\zeta & -\sin\zeta \\ \sin\zeta & \cos\zeta \end{pmatrix} \begin{pmatrix} \sigma_\ell & 0 \\ 0 & \alpha_\sigma\sigma_\ell \end{pmatrix} \begin{pmatrix} \cos\zeta & \sin\zeta \\ -\sin\zeta & \cos\zeta \end{pmatrix}. \tag{2.8}$$

Here, σ_ℓ is the conductivity in longitudinal direction, α_σ is the anisotropy ratio such that $\alpha_\sigma\sigma_\ell$ represents the conductivity in transverse direction, and ζ is the angle of longitudinal conductivity relative to the x-axis. Due to the spatial organisation of ion channels, ζ also corresponds to the local orientation of the tissue and those two parameters will be considered identical.

Using these three parameters, the conductivity tensor can be represented as an ellipse. The semi-major and semi-minor axes are set equal to the longitudinal and transverse conductivities, and the ellipse is rotated with the fibre direction angle. The radius of the ellipse in a certain direction is then equal to the effective conductivity in that direction. Figure 2.3 shows an example of an ellipse representation for a single node.

EGM Measurements

The unipolar EGM measurement setup consists of a regular lattice of $M_x \times M_y = M$ electrodes. This lattice is placed on the cardiac tissue, with an assumed constant cell to sensor height z. The distance between electrode m and node n is found as

$$r_{m,n} = \sqrt{(x_m - x_n)^2 + (y_m - y_n)^2 + z^2} \tag{2.9}$$

when the electrode thickness is assumed negligible (see also [12]). Each electrode indirectly measures the transmembrane potential of the area around the electrode. The resulting measured potential Φ_m for electrode m can be expressed as a function of the transmembrane current densities [13], and after discretisation results in

$$\Phi_m = \frac{\Delta x \Delta y}{4\pi\sigma_\mathrm{e}} \sum_{n=1}^{N} \frac{I_n}{r_{m,n}} \tag{2.10}$$

where σ_e is the extracellular conductivity constant and I_n denotes the transmembrane current density for the nth node, found from a discretisation of (2.5) at (x_n, y_n).

Local Activation Time

When a depolarisation wave passes through the tissue, each cell is activated at a different time. The local activation time is therefore not a parameter inherent to the tissue but a property of a specific

depolarisation wave, and can thus only be defined relatively within the time frame of a specific heartbeat. The local activation time τ of a cell is found from the transmembrane potential either as the instant a certain threshold is reached or as the instant the time derivative is maximal. In practice, however, transmembrane potentials are only known indirectly through the measured EGM potentials, and the local activation times have to be estimated. A number of different estimation methods exists [14], but one of the most common method is to use the instant the time derivative of the measured potential is minimal. This estimate leads to an $M_x \times M_y$ discrete, approximate activation map.

2.3. Tissue Conductivity Estimation Methods

Although estimating cardiac tissue parameters from epicardial electrograms is a complex and ill-posed inverse problem, several methods of solving this problem have been developed. This section describes two such methods and highlights the necessary underlying assumptions and simplifications. The first method is based around a compact matrix model (CMM) for electrograms and was created by Abdi *et al.* in 2019 [15]. The second method makes use of simultaneous confirmatory factor analysis (SCFA) [16] and was developed by Sun *et al.* in 2021 [17], [18].

Compact Matrix Model

The estimation method by Abdi *et al.* [15] aims to estimate the longitudinal conductivities and starts with the two-dimensional discretised monodomain model. The transmembrane potentials for all N nodes and T time instances are expressed as the $N \times T$ matrix $\boldsymbol{V}$, the measured potentials similarly for all M electrodes as the $M \times T$ matrix $\boldsymbol{\Phi}$, and the reciprocal distances $1/r_{m,n}$ from (2.9) as the $M \times N$ matrix $\boldsymbol{R}$. With these matrix representations, the EGM model of (2.10) can be reformulated as

$$\boldsymbol{\Phi} = \frac{\Delta x \Delta y}{4\pi\beta\sigma_{\mathrm{e}}} \boldsymbol{R} \boldsymbol{D}_\sigma \boldsymbol{V}. \tag{2.11}$$

The double spatial derivative operator $\boldsymbol{D}_\sigma$ is used to express the transmembrane current density in (2.10) in terms of the transmembrane potential using (2.5). This operator also contains the conductivity parameters.

When estimating the conductivity parameters from (2.11), computation of the transmembrane potential matrix is required. This process can be simplified by assuming that all action potentials have the same temporal shape but a different activation time [19], [20]. This means that the action potential of the nth node, $V_n(t)$, can be replaced by a stereotypical action potential $V_0(t - \tau_n)$ with the corresponding local activation time τ_n. The matrix $\boldsymbol{V}_\tau$ resulting from this substitution can then replace the true $\boldsymbol{V}$ in (2.11). The stereotypical action potential is obtained from the Courtemanche ionic current model, and the local activation times are estimated from the EGMs. For nodes not directly under electrodes, interpolation is used.

Finally, the linear dependency between the measured potential and longitudinal conductivity is highlighted by reformulating the measured potential as a vector where all the columns of $\boldsymbol{\Phi}$ are stacked to form a single vector of length MT. Vector $\boldsymbol{\sigma}_\ell$ contains the longitudinal conductivities for all N nodes. Using properties of the Khatri–Rao and Kronecker products, (2.11) can then be reformulated as

$$\mathrm{vec}(\boldsymbol{\Phi}) = \boldsymbol{M}_\tau(\zeta)\,\boldsymbol{\sigma}_\ell. \tag{2.12}$$

The mixing matrix $\boldsymbol{M}_\tau$ consists of all the known constants of (2.11), and depends nonlinearly on the fibre direction. The resulting equation, with a clear linear dependence between measured potentials and conductivity parameters, is known as the compact matrix model (CMM) for atrial electrograms.

To estimate the longitudinal conductivity values, the least squares difference between the measurements and model output is minimised. Both the anisotropy and fibre direction for each node are assumed to be known. An L1-norm regularisation term promotes a sparse solution with respect to an average conductivity value that is determined by prior knowledge. A nuclear norm (sum of singular values) regularisation term promotes spatial smoothness of the conductivity. The optimisation problem is solved using the Split Bregman method [21], which solves the problem iteratively by separating it into smaller problems and updating the estimates one at a time.

Simultaneous Confirmatory Factor Analysis

The estimation method by Sun *et al.* [17], [18] is based partly on the CMM method and similarly uses the discretised two-dimensional monodomain model. A stereotypical action potential is again assumed,

such that the action potential of node n can be approximated as a temporal convolution (denoted by $*$) of the stereotypical action potential $V_0(t)$ with a Dirac delta function:

$$V_n(t) \approx V_0(t - \tau_n) = \delta(t - \tau_n) * V_0(t). \tag{2.13}$$

Concatenating the Dirac delta functions for all N activation times into a vector, the M measured potentials at time t can be written as

$$\boldsymbol{\Phi}(t) = \frac{\Delta x \Delta y}{4\pi \beta \sigma_{\mathrm{e}}} \boldsymbol{R} \boldsymbol{D}_\sigma \boldsymbol{\delta}(t) * V_0(t) + \boldsymbol{U}(t) = \boldsymbol{h}(t) * V_0(t) + \boldsymbol{U}(t). \tag{2.14}$$

It is assumed that the electrodes measure some noise $\boldsymbol{U}(t)$ but no interference from neighbouring tissue. The mth element of $\boldsymbol{h}(t)$ can be seen as an impulse response from the nodes to the mth electrode. Using a short-time Fourier transform on (2.14) results in

$$\tilde{\boldsymbol{\Phi}}(k,l) = \tilde{\boldsymbol{h}}(k,l)\tilde{V}_0(k,l) + \tilde{\boldsymbol{U}}(k,l) \tag{2.15}$$

for frequency bin k and time frame l. Time frames are chosen such that each contains one heartbeat. The longitudinal conductivity and anisotropy ratio parameters are assumed to be constant across different frequencies and time frames (heartbeats).

These parameters can now be estimated using confirmatory factor analysis (CFA). CFA is a structural equation modelling technique that estimates parameters by reproducing an input covariance matrix [16]. For each frequency and time frame, two estimates of the power spectral density matrix of the measured potential can be formed. The first is based on the model of (2.15) using the unknown tissue parameters, the second is a maximum likelihood estimate using the measured data. The simultaneous CFA (SCFA) approach aims to minimise the Frobenius norms of the difference between these two power spectral density matrices, summed over frequency and time frames. Constraints on the optimisation parameters are included for robustness, ensuring that the target parameters fall into reasonable bounds set by prior knowledge. The optimisation problem is solved numerically using an interior-point algorithm.

Assuming appropriate conditions for both estimation methods, the SCFA method outperforms the CMM method [17], [18]. However, the two methods are based on different assumptions. The CMM method assumes that the fibre directions and anisotropy ratios are known before estimation. This reduces the applicability of the method to measurements where the tissue geometry is taken into account. The SCFA method estimates anisotropy ratios per node along with the main conductivities, but the fibre direction angle is assumed to be zero for all nodes. This not only requires the fibre direction to be smooth, but also forces measurements to be taken more strictly as the electrode array must be aligned with the tissue.

3

Effect of the Fibre Direction on Atrial Physiology

The fibre direction of atrial tissue determines the orientation of anisotropic conductivity and thus plays an important role in the physiology of the heart. The conductivity estimation methods highlighted in Chapter 2 either assume the fibre direction to be known, or require the electrode array to be aligned with the fibre direction. In this chapter, the effects of the fibre direction on atrial physiology and on the performance of conductivity estimation methods will be explored.

The two-dimensional conductivity tensor is composed of three parameters, either represented in the matrix form of (2.7) or in the eigendecomposition form of (2.8). The fibre direction appears in the latter expression and parametrises the eigenvectors. Due to the symmetrical nature of the conductivity tensor, the eigenvector matrix is a rotation matrix with the fibre direction as rotation angle. As would be expected intuitively, this means that a nonzero fibre direction simply rotates the conductivity properties with respect to the electrode array. The effect of this rotation depends on the anisotropy: a lower anisotropy ratio means that the fibre direction can influence the effective conductivity in a certain direction more heavily.

In the monodomain model of (2.6), the conductivity tensor appears in the spatial gradient term. When a cell is depolarised, the potential gradient that arises causes a transmembrane current to flow through neighbouring cells. This current raises the transmembrane potential of those cells until the activation threshold is reached. The fibre direction in the conductivity tensor therefore has a direct effect on the depolarisation wavefront orientation and thus on the activation times of the cells. A simulation example is presented in Figure 3.1, which shows simulated activation maps based on homogeneous, anisotropic tissue but with four different fibre directions. The activation times change considerably depending on the fibre direction, and elliptical wavefronts in the corresponding fibre directions can roughly be made out. The fibre direction therefore clearly impacts the local activation times.

Once a cell is depolarised, however, the dynamical behaviour of the cell is predominantly controlled by the ionic currents through the tissue. These ionic currents are independent of the potential gradient or the conductivity tensor. The fibre direction therefore only influences the activation times and not the temporal shape of the transmembrane potential. Figure 3.2a shows the transmembrane currents at node $n_x = 45$, $n_y = 1$ corresponding to the four simulations in Figure 3.1. These currents are approximately delayed versions of each other and have similar amplitude and shape. This is highlighted more clearly in Figure 3.2b, where the currents are shifted with their corresponding local activation time such that they overlap. This demonstrates that the fibre direction indeed barely affects the temporal shape of the transmembrane current (and, in extension, of the transmembrane potential) after activation.

The effect of the fibre direction on conductivity estimation methods is hard to quantify, both theoretically and experimentally. Due to the high nonconvexity of the estimation problems with respect to the fibre direction, estimation performances for different fibre directions are difficult to compare.

Considering a wrong fibre direction, and consequentially wrong activation times, causes model mismatch errors in the compact matrix model used in both the CMM and SCFA estimation methods. An

(a) $\zeta = 0 \, \mathrm{rad}$

(b) $\zeta = \frac{1}{4}\pi \, \mathrm{rad}$

(c) $\zeta = \frac{1}{2}\pi \, \mathrm{rad}$

(d) $\zeta = \frac{3}{4}\pi \, \mathrm{rad}$
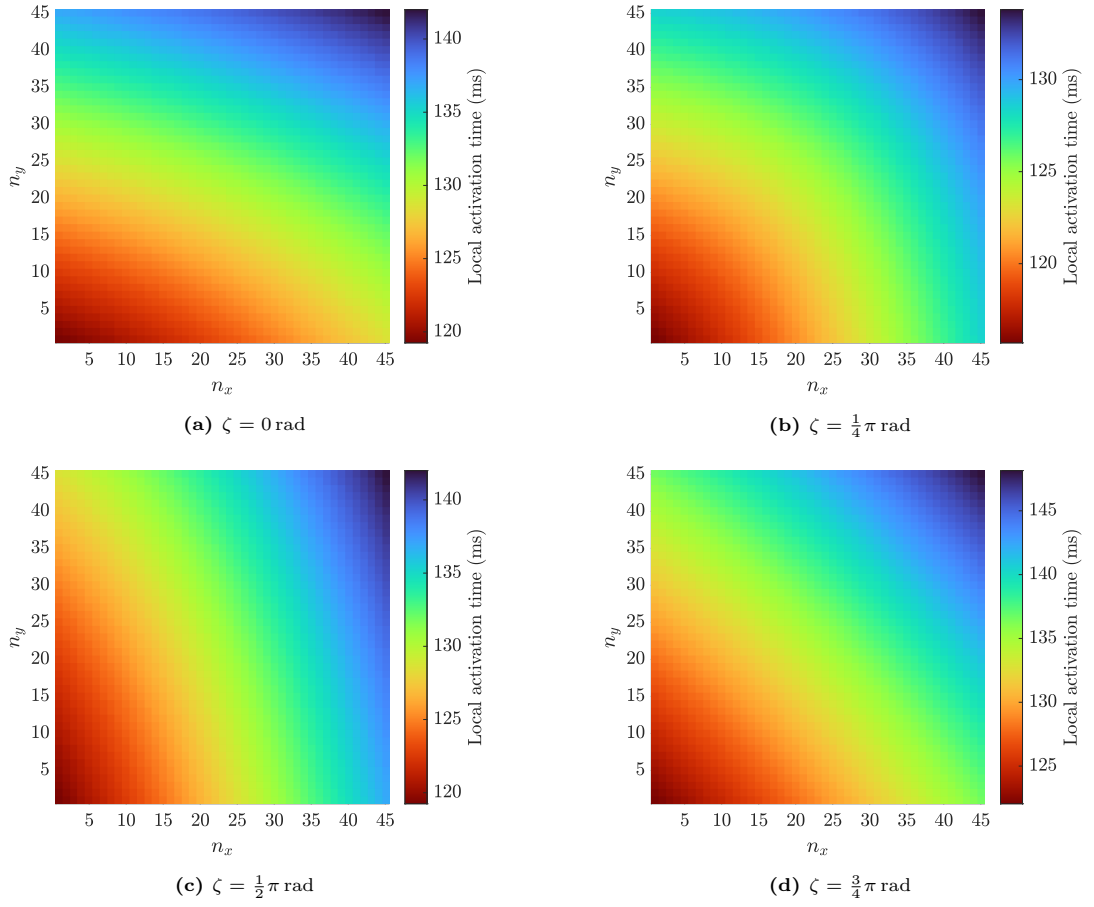
Figure 3.1: Simulated activation maps for homogeneous tissue with $\alpha_\sigma = \frac{1}{2}$ and different ζ.

(a)

(b)
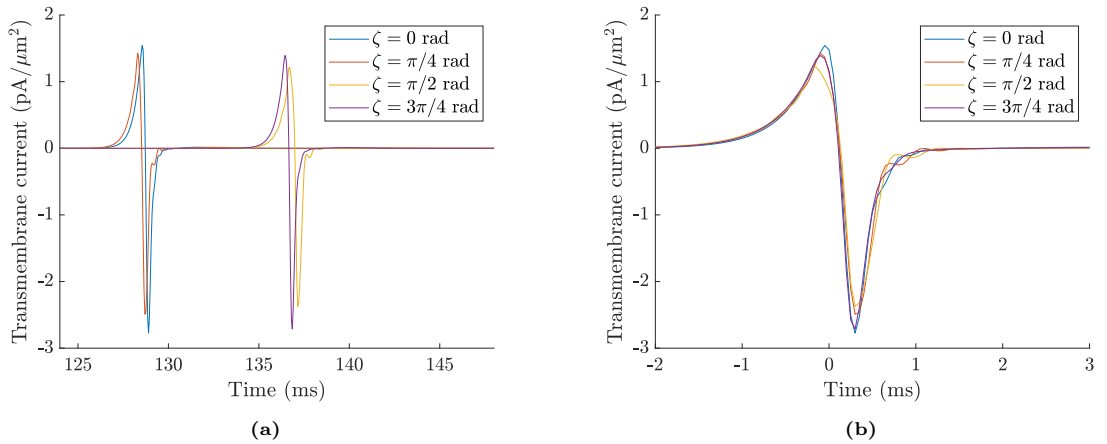
Figure 3.2: Simulated transmembrane current densities of a certain node for homogeneous tissue with $\alpha_\sigma = 0.5$ and different ζ, against time **(a)** within the time frame, **(b)** relative to the activation time of the node for each simulation.

error in the fibre direction $\mathcal{E}_\zeta$ translates to an error in the longitudinal conductivity of

$$\mathcal{E}_{\sigma_\ell} = \sigma_\ell(1 - \alpha_\sigma)\sin^2 \mathcal{E}_\zeta. \tag{3.1}$$

The conductivity error is higher for lower anisotropies because of the larger difference between longitudinal and transversal conductivity values. The largest conductivity error is found when the considered fibre direction is perpendicular to the true fibre direction, in which case the longitudinal and transversal directions are effectively interchanged. The model mismatch error from considering a wrong fibre direction can be expected to decrease the estimation performance, and knowing the fibre direction values as accurately as possible can therefore be beneficial.

<div align="right">

4

</div>
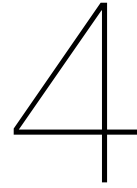
Fibre Direction Estimation

Because the fibre direction has a nontrivial influence on the potentials measured from an EGM, it can be useful to estimate the fibre direction based on EGM measurements. There are two ways to approach this problem. Firstly, the fibre direction can be estimated jointly with the conductivity by including it as an optimisation parameter. However, adding more unknowns to the optimisation problem without utilising additional information decreases the estimation accuracy. This might especially be true for the fibre direction, as it is a highly nonconvex parameter in the monodomain model in (2.6). Joint estimation of conductivity and fibre direction using existing methods might therefore not be the best approach.

Alternatively, the fibre direction can be estimated independently. This estimate can then either be used as a constant in a conductivity estimation method, or as an initial guess for a joint estimation. As demonstrated in Chapter 3, the fibre direction mostly influences the local activation times of cells. The independent estimation problem can therefore be reduced to using only activation maps of cells. One such method was developed by Roney *et al.* [22] and is based on elliptical wavefront fitting. This method requires the tissue to be homogeneous, such that the wavefronts are elliptical in shape. In the presence of conduction blocks, however, wavefronts break up. In these cases, elliptical wavefront fitting is no longer an accurate method. In this chapter, a novel fibre direction estimation method is presented that is more accurate for tissue with conduction blocks.

4.1. Conduction Slowness

An activation map of an area of cardiac tissue shows the propagation of a depolarisation wave. The velocity of the wavefront is known as the conduction velocity, and its reciprocal quantity is conduction slowness. Conduction slowness is an interesting wave property with a strong dependence on the conductivity parameters. Similarly to tissue conductivity, conduction slowness is orthotropic [23] and can be represented as an ellipse in the conduction slowness space. The orientation of this ellipse is the longitudinal conduction slowness direction ξ. This direction aligns with the transversal conductivity direction such that

$$\xi \perp \zeta. \tag{4.1}$$

The semiminor to semimajor axis ratio is the conduction slowness anisotropy ratio α_s, which is related to the conductivity anisotropy ratio as [24]

$$\alpha_s^2 = \alpha_\sigma. \tag{4.2}$$

The radius of the ellipse in the direction of a wavefront equals the effective conduction slowness of that wavefront. Figure 4.1 shows an example of the ellipse representation of the conduction slowness corresponding to the conductivity ellipse example in Figure 2.3.

The local conduction slowness of a node is a vector that can be found from the gradient of the corresponding activation map:

$$\boldsymbol{s}(x,y) = \begin{pmatrix} s_x(x,y) \\ s_y(x,y) \end{pmatrix} = \boldsymbol{\nabla}\tau(x,y). \tag{4.3}$$

13
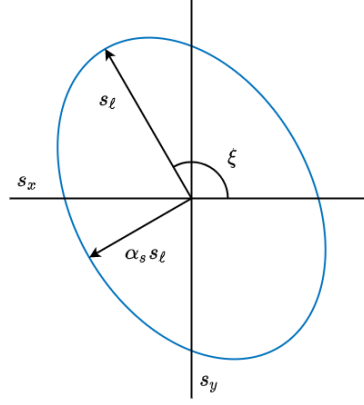
Figure 4.1: Ellipse representation of conduction slowness with $\alpha_s = \frac{1}{\sqrt{2}}$ and $\xi = \frac{2}{3}\pi$ rad.

Because activation maps are discrete, this gradient can be numerically approximated using the FDM. The local conduction slownesses can be represented as points in the conduction slowness space, and for a homogeneous area of tissue, these points roughly align with the aforementioned ellipse. The fibre direction and conductivity anisotropy ratio can therefore be estimated from an activation map by fitting a modelled ellipse to the conduction slowness points. This fitting problem is expressed mathematically as the least squares optimisation problem

$$
\min_{s_\ell, \alpha_s, \xi} \quad \sum_{n=1}^{N} \left(\|\boldsymbol{s}_n\| - \alpha_s s_\ell \left(\alpha_s^2 \cos^2 \left(\arctan \frac{s_{y,n}}{s_{x,n}} - \xi \right) + \sin^2 \left(\arctan \frac{s_{y,n}}{s_{x,n}} - \xi \right) \right)^{-\frac{1}{2}} \right)^2, \quad (4.4)
$$

where the sum of squared distances between the points for each node n and the modelled ellipse is minimised. The parameter s_ℓ is the longitudinal conduction slowness, which determines the scale of the fitted ellipse. Fibre direction and conductivity anisotropy ratio estimates can now be found from the optimisation parameter estimates using (4.1) and (4.2).

Two simulation examples are shown in Figure 4.2, corresponding to the first two activation maps in Figure 3.1. The local conduction slowness vectors are plotted as points, with relative area sizes corresponding to the amount of overlapping vectors. The magnitude of the vectors closely follow an elliptical shape, and the range of vector directions equals the range of wavefront directions present in the considered tissue area. A larger range of wavefront directions usually leads to a more accurate ellipse fit and therefore to more accurate estimates. The fitted ellipses, found from applying (4.4), are plotted as well. The resulting estimates are $\hat{\zeta} = 0.06\pi$ rad for Figure 4.2a and $\hat{\zeta} = 0.25\pi$ rad for Figure 4.2b, with $\hat{\alpha}_\sigma = 0.44$ for both.

When conduction blocks are present in the tissue, the elliptical wavefronts break up and wakes form behind the blocks. This effect can be observed in the simulated activation map in Figure 4.3. The corresponding conduction slowness space is shown in Figure 4.4. Although most local conduction slowness vectors still roughly follow the underlying ellipse, a notable number of outliers is present as well. Looking at a magnitude map of the local conduction slowness, shown in Figure 4.5, two main causes of these outliers can be seen. The first cause is the lower conductivity of the conduction blocks. Low conductivities cause high magnitudes of the local conduction slowness. All the high magnitude outliers are therefore concentrated at and closely around the conduction blocks. The second cause of the outliers is the thin trail of low magnitudes that can be observed at the centre of the wakes behind conduction blocks. This is where two wavefronts, coming from around each side of the block, collide. These collisions are characterised by a near-zero conduction slowness and thus cause low magnitude outliers.

The conduction block areas and the thin trails at the centre of their wakes produce unusable local conduction slowness vectors. However, most of the area in the wakes still behaves identical to the rest of the tissue, but with altered wavefront directions. As long as conduction blocks are not too large or prevalent, the number of unusable local conduction slowness vectors remains small. Outlier detection methods can be used to filter out magnitude outliers in the estimation process and the estimation performance will not be reduced too drastically.

(a) $\zeta = 0\,\mathrm{rad}$
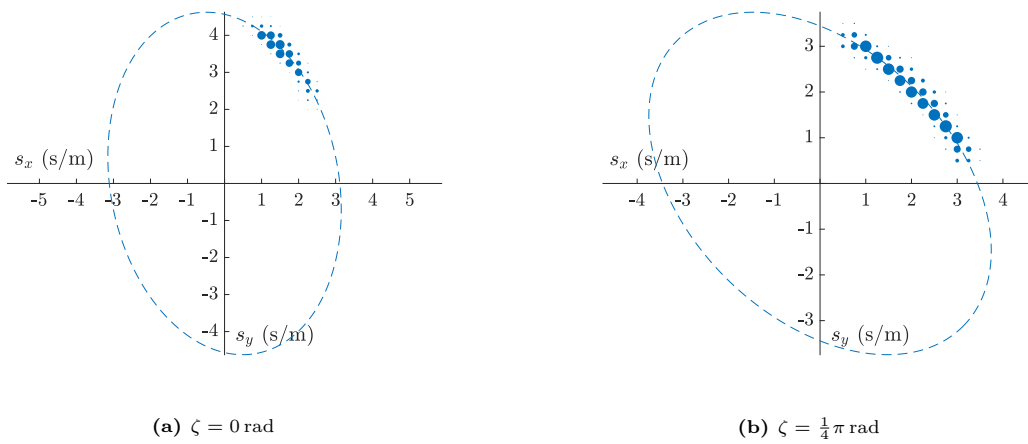

(b) $\zeta = \frac{1}{4}\pi\,\mathrm{rad}$

Figure 4.2: Local conduction slowness points and fitted ellipse (dashed line) corresponding to two of the activation maps in Figure 3.1.
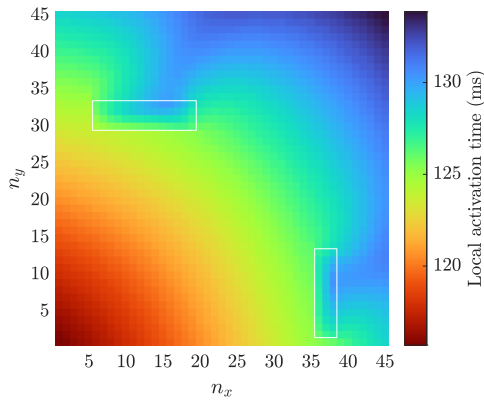

Figure 4.3: Simulated activation map for tissue with two conduction blocks (white outlines), with $\alpha_\sigma = \frac{1}{2}$ and $\zeta = \frac{1}{4}\pi\,\mathrm{rad}$.
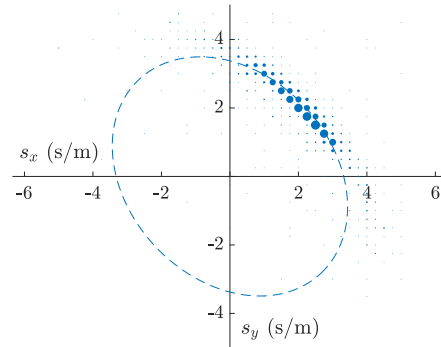
Figure 4.4: Local conduction slowness points and fitted ellipse (dashed line) corresponding to the activation map in Figure 4.3. Some outliers, with magnitudes up to $17\,\mathrm{s/m}$, are not visible here.
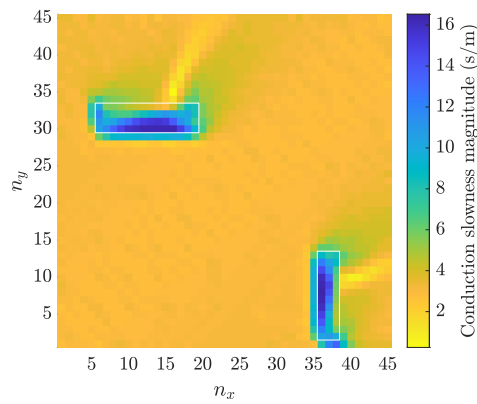
Figure 4.5: Magnitude map of the conduction slowness corresponding to Figure 4.3.
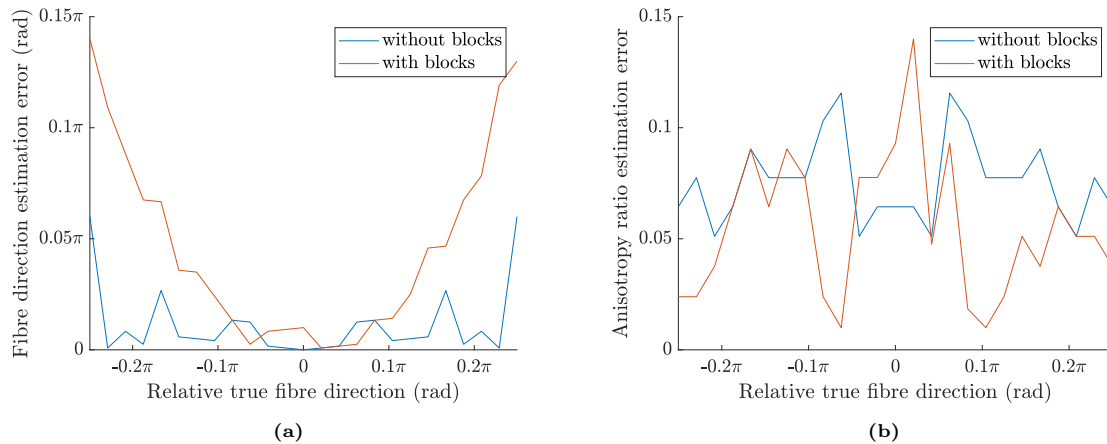
Figure 4.6: Absolute estimation errors for the **(a)** fibre direction and **(b)** conductivity anisotropy ratio, both in cases without conduction blocks and with two conduction blocks similar to the setup of Figure 4.3. The tissue has $\alpha_\sigma = \frac{1}{2}$ and a varying true fibre direction, indicated relative to the wave origin direction.

The final fibre direction estimation algorithm based on activation maps can now be described by the following steps:

1. find activation time estimates τ from measured potentials Φ;

2. calculate local conduction slowness vectors $\boldsymbol{s}$ using (4.3);

3. remove conduction slowness outliers, corresponding to conduction blocks, based on magnitude;

4. estimate conduction slowness parameters ξ and α_s using (4.4);

5. convert conduction slowness parameters to the fibre direction ζ and conductivity anisotropy ratio α_σ using (4.1) and (4.2).

4.2. Estimation Results

To test the estimation method, activation maps were simulated for tissue with a range of fibre directions, both without and with two conduction blocks (similar to the activation maps of Figures 3.1 and 4.3 respectively). The estimation algorithm was applied to these activation maps, and the resulting estimation performance is shown in Figure 4.6. For both the fibre direction and conductivity anisotropy ratio, the estimation performance is expressed as the absolute error, given by the absolute difference between the estimated and true parameter.

The fibre direction estimation performs well, especially in the case without blocks. Due to the symmetry of the ellipse, the absolute error is always between 0 rad and $\frac{1}{2}\pi$ rad. Guessing a fibre direction at random would therefore lead to an expected absolute error of $\frac{1}{4}\pi$ rad, which this method stays far below. The estimation performance is (roughly) independent of the absolute fibre direction and wave origin direction. A mismatch between these two directions, however, does influence the estimation performance significantly. This is because larger deviations lead to smaller ranges of wavefront directions present in the tissue area. The two examples of Figure 4.2 show this: Figure 4.2a corresponds to a mismatch of $\frac{1}{4}\pi$ rad and has a significantly smaller wavefront direction range than Figure 4.2b, corresponding to no mismatch. A smaller wavefront range makes the ellipse fitting process less accurate, which in turn decreases the estimation accuracy. This can be observed in Figure 4.6, where the absolute errors are plotted against the true fibre direction relative to the wave origin direction. In practice, only small deviations between fibre direction and wave origin direction would be expected, which favours smaller estimation errors for this method.

The conductivity anisotropy ratio estimation is not very accurate. The estimation error does not reach zero under any circumstance, but the estimated values are still within a decent range (compared to the maximum error of 0.5 in this simulation). The absolute estimation error does not seem to correlate much with the true fibre direction or with whether or not some conduction blocks are present.
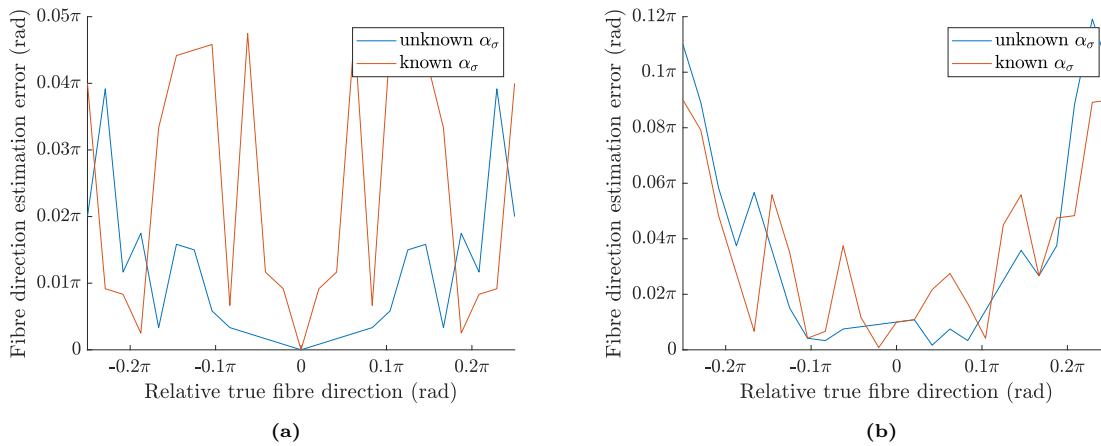
Figure 4.7: Absolute estimation errors for the fibre direction for tissue **(a)** without conduction blocks and **(b)** with two conduction blocks similar to the setup of Figure 4.3. The tissue has $\alpha_\sigma = \frac{1}{2}$ and a varying true fibre direction, indicated relative to the wave origin direction. Estimation errors are shown both for when α_σ is estimated and for when α_σ is known.

Known Anisotropy Ratio

In contrast to the fibre direction, the conductivity anisotropy ratio is a tissue parameter that is independent of the frame of reference of the measurement setup. Instead of estimating this parameter, it can also be assumed to be known beforehand, for example by using a value found in literature [25]. This value, converted to the conduction slowness anisotropy ratio with (4.2), can then be used as a known constant in (4.4) instead of treating it as optimisation parameter. This would remove an unknown in the optimisation step.

Figure 4.7 shows absolute estimation errors for the fibre direction, both for when the anisotropy ratio is estimated and for when the true anisotropy ratio is used as constant. On the average, using the true anisotropy ratio does not seem to improve the estimation performance. This can possibly be because the anisotropy ratio does not add much uncertainty in the optimisation of (4.4). Removing the unknown would therefore not lead to better estimates. Another possibility is that the used model of (4.2) is not accurate or not fully valid under conditions used in the simulation. This might also explain why the conductivity anisotropy ratio estimation error does not reach zero under any circumstance.

Activation Map Resolution

For the previous simulations, the activation times for all N nodes were used. In practice, however, activation times are estimated from the measured potentials. This leads to a lower spatial resolution, depending on the number of electrodes M. Figure 4.8 shows simulated absolute estimation errors for the fibre direction, for a decreasing spatial resolution. For tissue without blocks, the average error only slightly increases for lower resolutions. This is because the number of conduction slowness vectors has a smaller impact on the estimation performance than the range of vector directions, which is roughly preserved for lower resolutions. For tissue with conduction blocks, however, the decreased spatial resolution does have a considerable impact on the estimation performance. A decreased resolution blurs the activation times around the blocks, which means that relatively more conduction slowness vectors are affected by the blocks. Higher spatial resolution measurements therefore result in more accurate estimates, in particular when conduction blocks are present. The average conductivity anisotropy estimation performance is barely affected by the resolution of the activation map, except in the extreme case of a $M = 5 \times 5$ activation map for tissue with conduction blocks.

Aside from the spatial discretisation, time is also discretised. This means that the conduction slowness vectors can only take on values on a regular lattice in the conduction slowness space, which is visible in Figures 4.2 and 4.4. Increasing the temporal resolution also increases the conduction slowness resolution, such that the conduction slowness vectors more closely follow the underlying ellipse. However, as long as the temporal resolution is high enough to properly estimate the activation times, increasing the resolution does not have a significant impact on the estimation performance. The discretisation errors are roughly averaged out in the fitting process.
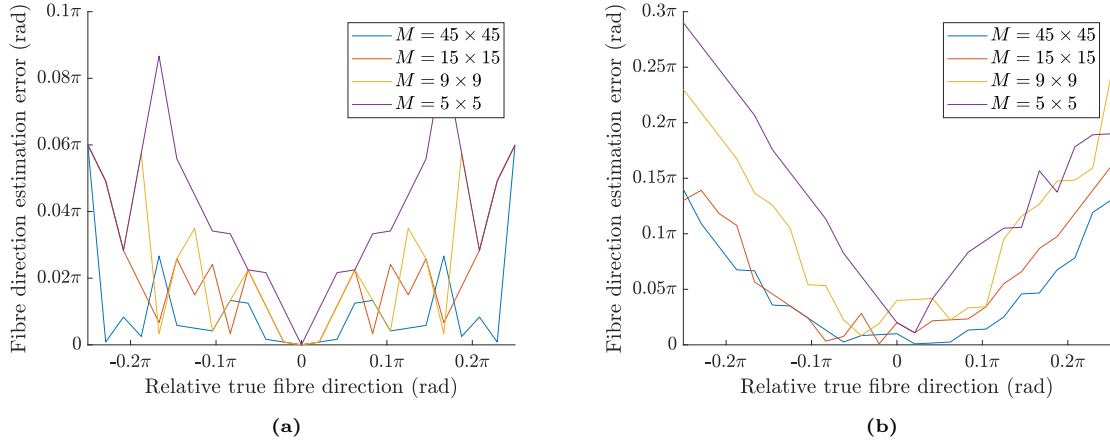
Figure 4.8: Absolute estimation errors for the fibre direction for tissue **(a)** without conduction blocks and **(b)** with two conduction blocks similar to the setup of Figure 4.3. The tissue has $\alpha_\sigma = \frac{1}{2}$ and a varying true fibre direction, indicated relative to the wave origin direction. A decreasing number of activation times M is used.
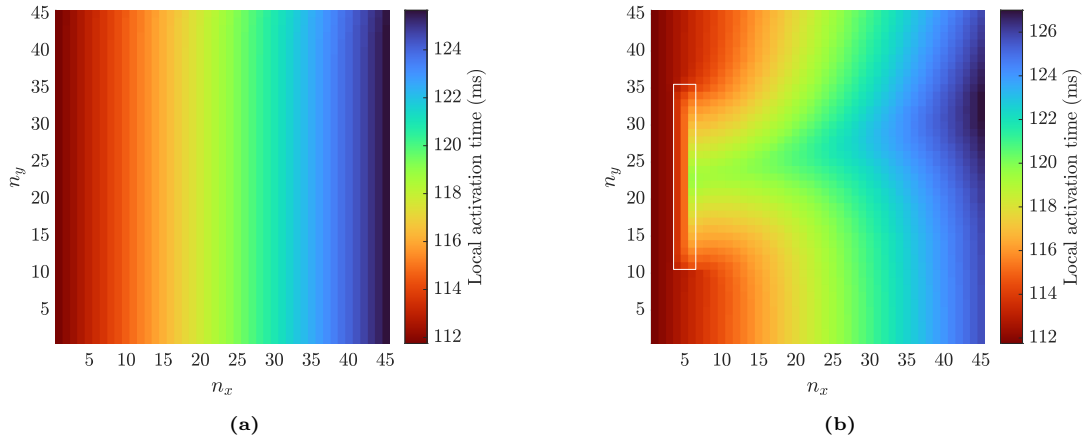

Figure 4.9: Simulated activation maps for a planar activation wave through tissue **(a)** without and **(b)** with a conduction block (white outlines), with $\alpha_\sigma = \frac{1}{2}$ and $\zeta = \frac{1}{6}\pi$ rad.

Planar Wavefronts

If an approximately planar activation wave propagates through homogeneous tissue, the range of wavefront directions present in the tissue is small. This leads to poor estimates. Sometimes, the presence of a conduction block can help to limit this problem. Although a conduction block introduces unusable conduction slowness outliers, it can also break up a planar wavefront causing a wider range of wavefront directions. Because the area around and behind the conduction block still follows the underlying conduction slowness ellipse, this increased wavefront direction range can be beneficial to the estimation. The presence of conduction blocks can therefore improve the estimation performance under certain circumstances with planar wavefronts.

An example simulation of a planar wavefront is shown in Figure 4.9, both for homogeneous tissue and for tissue with a conduction block. The corresponding conduction slowness points and fitted ellipse are shown in Figure 4.10. For the tissue without a conduction block, the range of wavefront directions is indeed small. The resulting estimates $\hat{\zeta} = 0.00$ rad and $\hat{\alpha}_\sigma = 0.64$ are poor due to this limited range. When a conduction block is present, however, the planar wavefront breaks up and the wavefront direction range is increased significantly. Even though some outliers are added, the resulting estimates $\hat{\zeta} = 0.15\pi$ rad and $\hat{\alpha}_\sigma = 0.51$ are highly accurate. This simulation example shows that the fibre direction estimation can indeed improve with the presence of conduction blocks for certain situations.
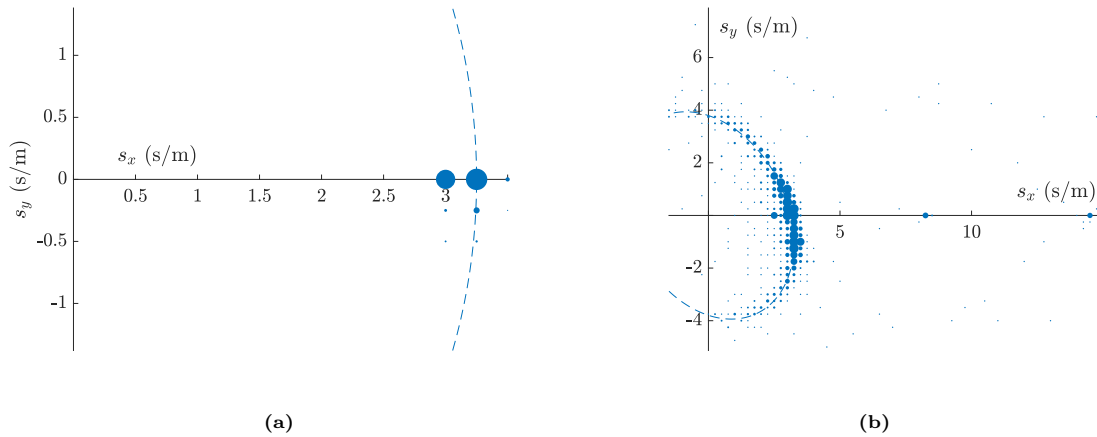
Figure 4.10: Local conduction slowness points and fitted ellipse (dashed line) corresponding to the two activation maps of Figure 4.9 respectively. Some outliers, with magnitudes up to 29 s/m, are not visible in **(b)**.

Inhomogeneous Estimation

Up until now, the tissue parameters were considered to be homogeneous, except for some possible conduction blocks. It is reasonable to assume that the conductivity anisotropy ratio and fibre direction usually do not vary much for a small area of tissue, such that only a single set of parameters needs to be estimated. It might, however, still be useful to be able to estimate those parameters inhomogeneously for different subareas within the measured area. This can be done trivially by applying the estimation algorithm separately for each subarea. The drawback to this approach is that the effective area used for each local estimation is decreased, leading to smaller ranges of wavefront directions available. Increasing the spatial resolution of the estimation therefore leads to less accurate estimates. More intricate methods of inhomogeneous estimation might be able to improve this trade-off.

4.3. Summarised Observations

Based on the numerous simulations performed for Section 4.2, some observations can be made about the performance of the estimation algorithm. The largest factor influencing the estimation accuracy is the range of wavefront directions present in the tissue area that is considered. A larger range leads to a more accurate ellipse fitting and in turn to a higher estimation accuracy. The range of available wavefront directions is mainly determined by the size of the considered tissue area and its closeness to the wave origin. The alignment between the fibre direction and wave origin direction also influences the wavefront direction range in this way, due to the anisotropic nature of the tissue. In case of approximately planar wavefronts, the presence of conduction blocks can also increase the wavefront direction range because of the wavefront breakup around the block. The spatial resolution of the used activation map does not influence the estimation accuracy much, except for when conduction blocks are present. For too low spatial resolutions, the activation times around blocks become blurred, decreasing the proportion of useful activation times and hindering outlier detection. The temporal resolution of the used activation map does not influence the estimation accuracy much as long as the resolution is high enough to properly estimate the activation times. The conductivity parameters can be estimated inhomogeneously by dividing the measurement area into smaller subareas, with a trade-off between spatial resolution of the estimates and their accuracy.

5

Conclusion

The fibre direction is a tissue parameter that determines the direction of longitudinal conduction of the tissue and appears in the spatial differential term of the monodomain equation. Through simulated experimental observations, based on the monodomain and Courtemanche models, it was concluded that the fibre direction almost exclusively influences the shape of the depolarisation wavefronts. This means that (only) the activation times of the cells are dependent on the fibre direction. Considering a wrong fibre direction can therefore lead to significant model mismatch errors when estimating the tissue conductivity using an estimation method like the CMM of SCFA methods. It can thus be useful to estimate the fibre direction.

The fibre direction can simply be included as an additional optimisation parameter in conductivity estimation methods, such that it is estimated jointly with the conductivity. This will, however, decrease the estimation accuracy because an additional, nonconvex unknown is added to the problem. A better strategy is therefore to estimate the fibre direction independently. Based on the aforementioned observations, this estimation can be performed using an activation map of the measured tissue area. A novel method was presented that estimates the fibre direction of atrial tissue based on conduction slowness. Starting from an activation map, local conduction slownesses can be calculated. Due to some interesting properties of the conduction slowness and its relation to conductivity, the fibre direction and conductivity anisotropy ratio of an area of tissue can be estimated from these local conduction slownesses. Numerous simulations were performed to test the estimation method under different circumstances. These simulations show that the method performs well (in relation to guessing at random) and is quite robust against the presence of conduction blocks. Reduced spatial resolution activation maps also barely affect the estimation accuracy, up to a reasonable limit.

A similar fibre direction estimation method has been developed by Roney *et al.* in 2019 [22]. This method estimates a fibre direction and anisotropy ratio by applying elliptical wavefront fitting to an activation map. The estimation accuracy of this method is adequate, as long as the area of tissue is homogeneous. When conduction blocks are present, the wavefronts break up around the blocks such that they are no longer elliptical. In these cases, the wavefront fitting method no longer works. Consequently, this method does not work well in combination with conductivity estimation algorithms like the CMM and SCFA algorithms, because their aim is to detect conduction blocks. The main goal of the estimation method presented in this thesis was to provide accurate estimates even in cases of tissue with conduction blocks. The performed simulations show that this goal has been achieved. The estimation method presented in this thesis is therefore a considerable improvement upon existing fibre direction estimation algorithms based on epicardial electrograms.

Although initial results of the fibre direction estimation method are promising, there are still a number of open questions concerning the algorithm itself and its applicability in certain scenarios. These open questions are provided below, together with some recommendations for possible future improvements of the method.

- **Improved outlier removal.** In this work, the removal of conduction slowness outliers corresponding to conduction blocks is based simply on the distribution of local conduction slowness magnitudes. Even though this approach was functional enough to present the estimation method

on a conceptual level, better outlier removal approaches might improve the estimation accuracy. This is especially true for tissue with a high proportion of conduction blocks.

- **Inhomogeneous estimation.** The estimation method presented was only applied on tissue with a homogeneous fibre direction and conductivity anisotropy ratio. Extending the method to estimate multiple sets of parameters, for different subareas within the measurement area, might be useful for inhomogeneous tissue. Although simply applying the method on smaller subareas gives a trade-off between spatial resolution and accuracy, more intricate approaches could improve the estimation on both fronts.

- **Extension to 3D.** In the tissue model used for the presented estimation method, the tissue was approximated as 2D. In practice, however, cardiac tissue consists of laminar sheets of myocytes. The fibre direction of these sheets rotates gradually throughout the tissue thickness [26]. Taking into account the third dimension and its special structure might improve the estimation accuracy.

- **Validation on physical data.** In this work, the presented estimation method was only tested on simulated EGMs. Despite the fact that the models used for the simulations have been shown to be accurate, the estimation method still has to be validated by applying it on physical data. This is complicated though, because physical data on epicardial measurements is limited and the corresponding true fibre directions are generally unknown.

References

[1] T. M. Munger, L.-Q. Wu, and W. K. Shen, "Atrial fibrillation," *J. Biomed. Res.*, vol. 28, no. 1, pp. 1–17, Jan. 2014.

[2] R. H. Clayton *et al.*, "Models of cardiac tissue electrophysiology: Progress, challenges and open questions," *Prog. Biophys. Mol. Biol.*, vol. 104, no. 1–3, pp. 22–48, Jan. 2011.

[3] F. B. Sachse, A. P. Moreno, G. Seemann, and J. A. Abildskov, "A model of electrical conduction in cardiac tissue including fibroblasts," *Ann. Biomed. Eng.*, vol. 37, no. 5, pp. 874–889, May 2009.

[4] D. A. Hooks, M. L. Trew, B. J. Caldwell, G. B. Sands, I. J. LeGrice, and B. H. Smaill, "Laminar arrangement of ventricular myocytes influences electrical behavior of the heart," *Circ. Res.*, vol. 101, no. 10, e103–e112, Nov. 2007.

[5] A. L. Hodgkin and A. F. Huxley, "A quantitative description of membrane current and its application to conduction and excitation in nerve," *J. Phys.*, vol. 117, no. 4, pp. 500–544, Aug. 1952.

[6] F. H. Fenton and E. M. Cherry, "Models of cardiac cell," *Scholarpedia*, vol. 3, no. 8, 2008, Art. no. 1868.

[7] S. Alonso, M. Bär, and B. Echebarria, "Nonlinear physics of electrical wave propagation in the heart: A review," *Rep. Prog. Phys.*, vol. 79, no. 9, Sep. 2016, Art. no. 096601.

[8] M. Courtemanche, R. J. Ramirez, and S. Nattel, "Ionic mechanisms underlying human atrial action potential properties: Insights from a mathematical model," *Amer. J. Physiol. Heart Circ. Physiol.*, vol. 275, no. 1, H301–H321, Jul. 1998.

[9] M. Potse, B. Dubé, J. Richer, A. Vinet, and R. M. Gulrajani, "A comparison of monodomain and bidomain reaction–diffusion models for action potential propagation in the human heart," *IEEE Trans. Biomed. Eng.*, vol. 53, no. 12, pp. 2425–2435, Dec. 2006.

[10] B. F. Nielsen, T. S. Ruud, G. T. Lines, and A. Tveito, "Optimal monodomain approximations of the bidomain equations," *Appl. Math. Comput.*, vol. 184, no. 2, pp. 276–290, Jan. 2007.

[11] Y. Coudière, Y. Bourgault, and M. Rioux, "Optimal monodomain approximations of the bidomain equations used in cardiac electrophysiology," *Math. Models Methods Appl. Sci.*, vol. 24, no. 6, pp. 1115–1140, Jun. 2014.

[12] B. Abdi, M. S. van Schie, N. M. S. de Groot, and R. C. Hendriks, "Analyzing the effect of electrode size on electrogram and activation map properties," *Comput. Biol. Med.*, vol. 134, Jul. 2021, Art. no. 104467.

[13] N. Virag *et al.*, "Study of atrial arrhythmias in a computer model based on magnetic resonance images of human atria," *Chaos*, vol. 12, no. 3, pp. 754–763, Sep. 2002.

[14] C. D. Cantwell, C. H. Roney, F. S. Ng, J. H. Siggers, S. J. Sherwin, and N. S. Peters, "Techniques for automated local activation time annotation and conduction velocity estimation in cardiac mapping," *Comp. Biol. Med.*, vol. 65, pp. 229–242, Oct. 2015.

[15] B. Abdi, R. C. Hendriks, A. van der Veen, and N. M. S. de Groot, "A compact matrix model for atrial electrograms for tissue conductivity estimation," *Comput. Biol. Med.*, vol. 107, pp. 284–291, Apr. 2019.

[16] T. A. Brown and M. T. Moore, "Confirmatory factor analysis," in *Handbook of structural equation modeling*, R. H. Hoyle, Ed. New York, NY, USA: Guilford, 2012.

[17] M. Sun, N. M. S. de Groot, and R. C. Hendriks, "Cardiac tissue conductivity estimation using confirmatory factor analysis," *Comput. Biol. Med.*, vol. 135, Aug. 2021, Art. no. 104604.

[18] M. Sun, N. M. S. de Groot, and R. C. Hendriks, "Joint cardiac tissue conductivity and activation time estimation using confirmatory factor analysis," *Comput. Biol. Med.*, vol. 144, May 2022, Art. no. 105393.

[19] M. S. Spach, W. T. Miller III, P. C. Dolber, J. M. Kootsey, J. R. Sommer, and C. E. Mosher Jr., "The functional role of structural complexities in the propagation of depolarization in the atrium of the dog: Cardiac conduction disturbances due to discontinuities of effective axial resistivity," *Circ. Res.*, vol. 50, no. 2, pp. 175–191, Feb. 1982.

[20] P. C. Franzone, L. Guerri, M. Pennacchio, and B. Taccardi, "Anisotropic mechanisms for multiphasic unipolar electrograms: Simulation studies and experimental recordings," *Ann. Biomed. Eng.*, vol. 28, no. 11, pp. 1326–1342, Nov. 2000.

[21] T. Goldstein and S. Osher, "The split Bregman method for L1-regularized problems," *SIAM J. Imag. Sci.*, vol. 2, no. 2, pp. 323–343, 2009.

[22] C. H. Roney *et al.*, "A technique for measuring anisotropy in atrial conduction to estimate conduction velocity and atrial fibre direction," *Comput. Biol. Med.*, vol. 104, pp. 278–290, Jan. 2019.

[23] T. Sano, N. Takayama, and T. Shimamoto, "Directional difference of conduction velocity in the cardiac ventricular syncytium studied by microelectrodes," *Circ. Res.*, vol. 7, no. 2, pp. 262–267, Mar. 1959.

[24] L. Clerc, "Directional differences of impulse spread in trabecular muscle from mammalian heart," *J. Phys.*, vol. 255, no. 2, pp. 335–346, Feb. 1976.

[25] B. M. Johnston and P. R. Johnston, "Approaches for determining cardiac bidomain conductivity values: Progress and challenges," *Med. Biol. Eng. Comput.*, vol. 58, no. 12, pp. 2919–2935, Dec. 2020.

[26] G. B. Sands, D. A. Gerneke, D. A. Hooks, C. R. Green, B. H. Smaill, and I. J. Legrice, "Automated imaging of extended tissue volumes using confocal microscopy," *Microsc. Res. Techn.*, vol. 67, no. 5, pp. 227–239, Aug. 2005.

A
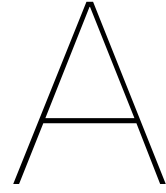
SITB 2022 Abstract

For the 42nd WIC Symposium on Information Theory and Signal Processing in the Benelux (SITB 2022), an extended abstract about the estimation method presented in this thesis was written and submitted. A poster presentation was subsequently held on 1 June. A copy of the abstract is included below.

Estimation of Atrial Fibre Direction Based on Activation Maps

Johannes W. de Vries, Richard C. Hendriks and Miao Sun

Circuits and Systems (CAS) Group, Delft University of Technology, The Netherlands

{J.W.deVries, R.C.Hendriks, M.Sun}@tudelft.nl

Abstract

Contractions of the atria are triggered by action potentials that are generated in the sinoatrial node and propagate through the atrial tissue. The propagation is dependent on the electrical conductivity of the tissue, which is generally orthotropic with a longitudinal orientation along the atrial fibre direction. Areas of impaired conductivity give rise to irregular wavefronts, which can lead to heart rhythm disorders such as atrial fibrillation. Being able to estimate the conductivity parameters from an epicardial electrogram (EGM) is therefore an important tool in diagnosing and treating these disorders. Several estimation methods have recently been developed, such as the compact matrix model by Abdi *et al.* and simultaneous confirmatory factor analysis by Sun *et al*. However, both methods assume the fibre direction relative to the sensor array to be known before estimation.

The fibre direction parametrises the effective conductivity in a direction and thus directly influences the shape of the activation wavefronts. Once a cell is activated, however, a stereotypical action potential can be assumed independent of the conductivity. Under this assumption, the fibre direction only influences the activation times of the cells. The fibre direction can therefore be estimated from an activation map, found as the moments of steepest descent for each electrode of an EGM. Current methods are based on fitting ellipses to the wavefronts in activation maps, which has a severely decreased performance for irregular wavefronts due to conduction blocks.

This work present a novel method to estimate the fibre direction and conductivity anisotropy from activation maps, in order to improve these estimates in the presence of conduction blocks. The method is based on the reciprocal conduction velocity (or conduction slowness), a vector field that can be calculated from an activation map using the finite difference method. Representing these vectors as coordinates, the resulting points roughly follow an ellipse whose orientation is perpendicular to the fibre direction. The ratio of the semimajor and semiminor axes of this ellipse is equal to the square root of the conductivity anisotropy ratio. These two parameters can therefore be estimated from the ellipse that results as the least squares fit of the conduction slowness vectors.

Activation maps were simulated for anisotropic tissue with varying fibre directions, both with and without conduction blocks. The absolute estimation errors for these simulations are shown in the left and right figures below for the fibre direction and conductivity anisotropy ratio respectively. These errors are plotted against the true fibre direction relative to the direction of the activation wave propagation. These results show that the method can accurately estimate the fibre direction for homogeneous tissue. In case of multiple conduction blocks, the performance is a bit worse but still relatively accurate (to within 0.1π rad most of the time). The anisotropy ratio is estimated accurately for both cases.